

To appear in ApJS, Spitzer Special Issue

The IRAC Shallow Survey

P. R. Eisenhardt¹, D. Stern¹, M. Brodwin¹, G. G. Fazio², G. H. Rieke³, M. J. Rieke³,
M. W. Werner¹, E. L. Wright⁴, L. E. Allen², R. G. Arendt⁵, M. L. N. Ashby², P. Barmby²,
W. J. Forrest⁶, J. L. Hora², J.-S. Huang², J. Huchra², M. A. Pahre², J. L. Pipher⁶,
W. T. Reach⁷, H. A. Smith², J. R. Stauffer⁷, Z. Wang², S. P. Willner², M. J. I. Brown⁸,
A. Dey⁸, B. T. Jannuzi⁸, and G. P. Tiede⁹

ABSTRACT

The IRAC shallow survey covers 8.5° in the NOAO Deep Wide-Field Survey in Boötes with 3 or more 30 second exposures per position. An overview of the survey design, reduction, calibration, star-galaxy separation, and initial results is provided. The survey includes $\approx 370,000$, $280,000$, $38,000$, and $34,000$ sources brighter than the 5σ limits of 6.4, 8.8, 51, and $50 \mu\text{Jy}$ at 3.6, 4.5, 5.8, and $8 \mu\text{m}$ respectively, including some with unusual spectral energy distributions.

Subject headings: surveys — infrared: stars — infrared: galaxies

¹Jet Propulsion Laboratory, California Institute of Technology, MS 169-327, 4800 Oak Grove Drive, Pasadena, CA, 91109; e-mail: peisenhardt@sirtfweb.jpl.nasa.gov

²Harvard-Smithsonian Center for Astrophysics, 60 Garden St., Cambridge, MA 02138

³Steward Observatory, University of Arizona, Tucson, AZ, 85721

⁴University of California, Los Angeles, CA 90095-1562

⁵NASA Goddard Space Flight Center, Greenbelt, MD 20771

⁶University of Rochester, Rochester, NY 14627

⁷*Spitzer* Science Center, California Institute of Technology, Pasadena, CA 91125

⁸National Optical Astronomy Observatory, Tucson, AZ, 85726-6732

⁹Bowling Green State University, Bowling Green, OH, 43403

1. Introduction

The million-fold lower background seen at infrared wavelengths in space means that even brief exposures with a modest aperture telescope like the *Spitzer Space Telescope* probe vastly larger volumes than are possible from the ground. For objects distributed uniformly in Euclidean space, the number of sources detected is maximized by observing a given field only long enough to become background limited, and to reduce repositioning overheads to 1/3 of the observing time. For uniform density sources observable to cosmological (non-Euclidean) volumes, the advantage of short exposures is greater. Such considerations motivated the IRAC shallow survey (*Spitzer* program number 30), which detects sources in the L -band $\approx 8,000\times$ faster than did Hogg et al. (2000) using Keck, while reaching $5\times$ deeper. The 23 hour *Infrared Space Observatory* observations at $6.7\mu\text{m}$ of Sato et al. (2003) detected sources a few times fainter than does the 90 second IRAC shallow survey at 5.8 and $8.0\mu\text{m}$, but at a rate several hundred times slower. The logical endpoint of this approach is an all-sky survey such as that planned by the *Wide-field Infrared Survey Explorer* (Eisenhardt & Wright 2003).

A major scientific driver for the IRAC shallow survey is the detection of galaxy clusters at $z > 1$ via the redshifted $1.6\mu\text{m}$ peak in galaxy spectral energy distributions (SEDs). Extending the evolution observed in the K -band in clusters to $z \sim 1$ (de Propris et al. 1999), we expect to detect cluster galaxies fainter than L^* at $z = 2$ at 3.6 and $4.5\mu\text{m}$. Much of the signal for photometric redshifts, which increase the contrast of such clusters, derives from the 4000\AA break or from the Balmer decrement. Hence deep complementary optical imaging is needed, and near-IR imaging is also helpful. The NOAO Deep Wide-Field Survey (hereafter NDWFS; Jannuzi & Dey 1999) meets this need with imaging in B_W , R , I , J , and K_s , and the 9.3° NDWFS Boötes region in particular has both high Galactic and high ecliptic latitude, providing low backgrounds for *Spitzer* imaging. The field center is near $\alpha = 14^{\text{h}}32^{\text{m}}06^{\text{s}}$, $\delta = +34^\circ16'47''$ (J2000). Observations of the Boötes field have also been completed in the radio (de Vries et al. 2002), in the far-IR with MIPS on *Spitzer*, in the near-IR with FLAMINGOS (Elston et al. 2004), and in the X-ray with ACIS on *Chandra* (Murray et al. 2004; Kenter et al. 2004). Far-UV observations with *GALEX* are underway.

The shallow survey team plans to address many other astrophysical objectives using these datasets, ranging from identifications and size estimates for high ecliptic latitude asteroids from $8\mu\text{m}$ thermal emission, to foreground subtraction for detection of fluctuations in the $1 - 3\mu\text{m}$ cosmic background due to $\text{Ly}\alpha$ from Population III objects at $z \sim 15$ (e.g., Cooray et al. 2004).

2. Observing Strategy and Data Processing

To achieve reasonable reliability, the survey design follows Clyde Tombaugh’s admonition to obtain at least three observations at each location. This results in a total of 17,076 separate $5' \times 5'$ images in the four IRAC bands. The 30s frame time used provides background-limited or nearly background-limited data in all four IRAC channels, and dominates the ~ 10 s needed to reposition by one IRAC field.

The 45 Astronomical Observation Requests (AOR’s) making up the shallow survey were executed during the 3rd IRAC campaign, on UT 2004 Jan 10 – 14. The survey area was split into 15 “groups”, each of which was observed three times with at least 2 hours between observations to ensure that asteroids could be reliably identified. The observation strategy incorporates several elements to facilitate self-calibration of the data (e.g., Fixsen, Moseley, & Arendt 2000): (i) *dithering*: each AORs starts at a different point in the small-scale cycling dither table; (ii) *offsets*: relative to the first AOR of each group, subsequent AOR revisits to a group are shifted by 1/3rd of the $290''$ step size used by our mapping; and (iii) *cadencing*: for large groups which are rectangular grids, revisits cover the same area with a different step size. For example, the first AOR of the first group uses an 8×12 grid map, while the revisits use a 9×12 and a 8×13 grid map. These strategies increase the intra-pixel correlations, providing a better self-calibration figure of merit (Arendt, Fixsen, & Moseley 2000).

A version 1 reduction was created using the basic methodology of the IRAC pipeline (IRAC Data Handbook, ver. 1.0; <http://ssc.spitzer.caltech.edu/irac/dh/>), with a few additional steps. Residual pattern noise in the images was removed by subtracting a median combination of the images for each AOR. Independent median images were constructed for each amplifier of each detector, with zero DC level to preserve the “sky” value of the images. A remaining “jailbar” pattern in the images (which was worst for $5.8\mu\text{m}$) was removed by adding a small constant to the image from each amplifier so that a detector’s four output amplifiers have equal median “sky” values. A correction for some of the known IRAC array artifacts associated with bright stars (mux-bleed and column pulldown) was applied.

Additional processing was needed for the $5.8\mu\text{m}$ data because these frames suffered obvious heightened systematic effects. A secondary median-combined delta-dark frame was generated and applied for the first $5.8\mu\text{m}$ image taken in each AOR. Finally an additive offset was applied to normalize the sky values in each individual $5.8\mu\text{m}$ image to the median of all $5.8\mu\text{m}$ images. This step removed any information at $5.8\mu\text{m}$ about structure larger than one IRAC field, but was needed to remove systematic trends within and between AORs.

The processed frames were combined into a single image for each channel using the SSC MOPEX software, after some experimentation with cosmic ray rejection parameters

and comparison with alternate reduction software. The output pixel scale of the mosaiced image is $\sqrt{2}$ smaller than the input pixel scale, and the output orientation was rotated $\sim 45^\circ$, following the recommendation of van Dokkum et al. (2000). Fig. 1 (Plate X) illustrates the full shallow survey mosaic at $4.5\mu\text{m}$, with various interesting sources highlighted.

3. Photometry

Source detection and photometry was carried out using SExtractor (Bertin & Arnouts 1996) in areas with at least 3 exposures (listed in Table 1). Unless otherwise noted, Vega-relative magnitudes are used throughout. Photometry was measured in $3''$ and $6''$ diameter apertures, and using the SExtractor “MagAuto” (roughly an isophotal magnitude, indicated by the subscript “auto”). Aperture magnitudes were corrected to the 10 pixel radius ($24''.4$ diameter) calibration diameter using values determined by the IRAC instrument team. For stars, SExtractor MagAuto values agreed with these aperture-corrected values to ~ 0.1 mag.

Table 1 gives the survey depths from the standard deviation of randomly-located $3''$ and $6''$ apertures, and saturation limits from inspection of bright star radial profiles in single exposure mosaics. While we believe the sources detected at 5σ in $3''$ apertures to be generally reliable, the more conservative $6''$ values are used hereafter unless otherwise specified.

The IRAC zeropoints, provided by the SSC, have a reported absolute calibration accuracy better than 10%. As a check, the IRAC sources were matched with 2MASS observations of the field, yielding $\approx 12,000$ matches per IRAC band. Sources with $J - K \leq 0.5$ are expected to be spectral-type K0V (or G2III) and earlier stars (Johnson 1966; Bessell & Brett 1988); the bluest nearby galaxies have $J - K > 0.7$ (Jarrett et al. 2003). Most stars should have close to zero color in IRAC bands (in the Vega system), as these wavelengths sample the Rayleigh-Jeans tail. Fig. 2 plots 2MASS to IRAC colors for the 2MASS $J - K \leq 0.5$ sources. These sources average $K - [3.6] = 0.09$, while the other IRAC bands are within 0.03 mag of the expected zero color. Bessell & Brett (1988) find that stars of spectral type B8V through K0V have $K - L$ colors of -0.03 to $+0.06$ and $K - M$ colors of -0.05 to $+0.03$. We conclude that the IRAC zeropoints are accurate at the 10% level.

4. Star-Galaxy Separation

Stars dominate the number counts for $m < 14$ in all IRAC bands (Fazio et al. 2004), so accurate identification of stars is necessary to avoid large errors in bright galaxy counts. Fig. 3 shows that morphological identification of stars with $[3.6] < 15$ is practical. Sources

with $-0.25 < [3.6]_{3''} - [3.6]_{\text{auto}} < 0.2$ and $[3.6]_{\text{auto}} < 15.25$ were counted as stars by Fazio et al. (2004), while those with $[3.6]_{3''} - [3.6]_{\text{auto}} < -0.25$ were rejected as probable cosmic rays. For unsaturated 4.5, 5.8, or $8\mu\text{m}$ sources with $[3.6] < 10.25$, a similar concentration criterion was used in the relevant filter. Because $3.6\mu\text{m}$ classification was used, the effective area for number counts at $m < 15$ is reduced to 8.06, 8.50, and 8.07sq° at 4.5, 5.8, and $8\mu\text{m}$. Objects with $m < 15$ at 4.5, 5.8, and $8\mu\text{m}$ but with $[3.6] \geq 15.25$ were counted as galaxies. For each wavelength, the brightest two magnitude bins of objects classified as galaxies by these criteria were individually inspected, and in some cases reclassified as stars or artifacts. At $5.8\mu\text{m}$, the fraction of bright artifacts was significant.

In the present paper we identify stars by concentration for $[3.6] < 15.0$, and via optical + IRAC photometry for fainter objects. A clear sequence of stars with $(B_W - I) > 2(I - [3.6]) - 1.65$ is evident (Fig. 5a), analogous to the *BIK* sequence identified by Huang et al. (1997). However, ~ 0.5 mag redder in $I - [3.6]$ than this criterion, a secondary sequence appears, containing roughly 40% as many stars. These are likely to be giant stars (Johnson 1966, Bessell & Brett 1988), and we label morphologically compact $3.6\mu\text{m}$ sources with $-1.65 > (B_W - I) - 2(I - [3.6]) > -3.35$ using yellow star symbols elsewhere in Fig. 4 and 5. Together dwarf and giant stars account for $\approx 17\%$ of 3.6 and $4.5\mu\text{m}$ sources in this survey.

5. Color-Magnitude and Color-Color Relations

To assess the general characteristics of the survey data, we have constructed a variety of color-magnitude and color-color plots, examples of which are illustrated in Fig. 4 and 5. In the released NW 1.2sq° of the NDWFS Boötes field, optical photometry was measured for IRAC shallow survey sources, and limits of $I = 24$ and $B_W = 26.7$ were used. Photometry for objects with $I < 16$ or $B_W < 17$ was not used because of saturation effects. Absolute astrometry for the shallow survey (calibrated to 2MASS) and the NDWFS (calibrated to the USNO-A2.0) in this region agrees to within $0.3''$ rms.

The diagonal edges which bound the data at lower left and upper right in Fig. 4 arise from the saturation and 2σ limits respectively in the bluer band. Fig. 4b shows a similar feature bounding the red symbols, corresponding to the $[3.6] < 15$ morphological classification limit, and this limit appears as a vertical edge in Fig. 4d. The number of objects redder than the 2σ limits are listed as a function of magnitude along the top axes in Fig. 4. Each such red object was inspected visually to confirm its reality when there were less than 100 in a magnitude bin. For magnitude bins with 100 or more objects redder than the limit, a representative subsample was inspected and used to provide a rough correction ($< 10\%$ in all cases) to remove spurious objects from the listed numbers.

6. Initial Results

An initial attempt at identifying $z > 1$ clusters used $F_\nu(4.5)/F_\nu(3.6) > 1$, based on the rest frame $1.6\mu\text{m}$ bump moving from the 3.6 to the $4.5\mu\text{m}$ channel. Fig. 1 illustrates a $400'' \times 400''$ region where the density of such objects is particularly high. Spectroscopic confirmation of such candidate clusters is clearly necessary.

The nearly horizontal edge at $I - [3.6] \sim 1$ in Fig. 4d appears to arise from an absence of stars bluer than this color in this field (cf Fig. 5a). A stellar sequence is apparent in most panels in Fig. 4 and 5, but a sequence of compact $3.6\mu\text{m}$ sources (red symbols) appears in Fig. 4a, 4b, and 5c with different colors than the dwarf and giant stars noted in §5. Preliminary spectroscopy of unresolved sources outside the stellar color loci suggests they are a mixture of broad-lined quasars and starburst galaxies. We find ≈ 300 such IRAC-selected objects in the released 1.2° corner of the NDWFS. It is premature to assess what fraction of these candidates are quasars, but it is noteworthy that the Sloan Digital Sky Survey finds a surface density of only 15 quasars/ $^\circ$ with $i^* \leq 19.1$ (Richards et al. 2002).

Finally, we give an illustration of the possibilities and challenges of identifying rare objects in the IRAC shallow survey. Using the released 1.2° portion of the NDWFS, a search was carried out for objects bright enough at $8\mu\text{m}$ for IRS short-low spectroscopy (taken as 0.35 mJy), but which are extremely challenging for optical spectroscopy (taken as $I \geq 24$). The vast majority of the 678 sources in this region with $8\mu\text{m}$ fluxes above 0.35 mJy are real, but selecting for unusual colors enhances the probability of spurious sources. Visual examination of the 19 candidates with $I \geq 24$ showed most were attributable to cosmic rays or scattered light from bright stars in the $8\mu\text{m}$ data. We therefore also required that they also be identifiable at 3.6 or $4.5\mu\text{m}$. This reduced the number of candidates to 4, of which the faint or absent I flux for 2 could be attributed to problems with the I data. The remaining two objects are deemed reliable. Fig. 6 shows the SED for one of these (the other is similar), together with some model spectra normalized at $8\mu\text{m}$.

How can we account for the properties of these objects? Their $8\mu\text{m}$ to $0.8\mu\text{m}$ flux ratio is > 500 , a spectral index of > 2.7 . One possibility is that these are relatively nearby starburst galaxies, whose $8\mu\text{m}$ flux is enhanced by $7.7\mu\text{m}$ PAH emission. The $z = 0$ model spectrum of Arp 220 from Devriendt, Guiderdoni, & Sadat (1999) illustrates this, but fails to match the observed I flux limit, needing an additional $A_I \sim 2$, equivalent to $A_V \sim 4$. The same model at $z = 1.4$ places rest $3.3\mu\text{m}$ emission at $8\mu\text{m}$ observed, with a similar mismatch at I . However in this case the A_V equivalent is only ~ 1 mag, because observed I samples rest $0.32\mu\text{m}$. The luminosity would be comparable to that of the ULIRG HR10 (ERO J164502+4626.4), i.e. in excess of $10^{12}L_\odot$ (Dey et al. 1999). The dashed line in Fig. 6 shows a quasar at $z = 1$ with $A_V \sim 3$ from Polletta et al. (2000) which matches the

the IRAC data well, but again additional reddening is needed to match the I limit. This spectrum matches the reddest AGN found by 2MASS. A final, less likely possibility is a quasar at $z > 6$ in which the Ly α forest suppresses observed light below $1\mu\text{m}$, as illustrated by the SDSS composite quasar spectrum in Fig. 6 from Vanden Berk et al. (2001). However Fan et al. (2003) find only ~ 1 such quasar per 500 square degrees.

Followup observations with *Spitzer's* Infrared Spectrograph are likely to reveal which of these possibilities is correct, or whether these objects represent some new phenomenon. The large volume probed by the IRAC shallow survey data will allow the discovery of many more objects with unusual colors.

We thank H. Spinrad and S. Dawson for providing spectroscopy of IRAC-selected quasar candidates. This work is based on observations made with the *Spitzer Space Telescope*, which is operated by the Jet Propulsion Laboratory, California Institute of Technology under NASA contract 1407. Support was provided by NASA through an award issued by JPL/Caltech. The NDWFS would not have been possible without support from NOAO, which is operated by the Association of Universities for Research in Astronomy under a cooperative agreement with the National Science Foundation (NSF). This publication makes use of data products from the Two Micron All Sky Survey, which is a joint project of the U. of Massachusetts and the Infrared Processing and Analysis Center/Caltech, funded by NASA and the NSF.

REFERENCES

- Arendt, R. G., Fixsen, D. J., & Moseley, S. H. 2000, ApJ, 536, 500
- Bertin, E. & Arnouts, S. 1996, A&AS, 117, 393
- Bessell, M.S. & Brett, J.M. 1988, PASP, 100, 1134
- Cooray, A., Bock, J. J., Keatin, B., Lange, A. E., & Matsumoto, T. 2004, ApJ, 606, 611
- de Propriis, R., Stanford, S. A., Eisenhardt, P. R. M., Dickinson, M., & Elston, R. 1999, AJ, 118, 719
- de Vries, W. H., Morganti, R., Röttgering, H. J. A., Vermeulen, R., van Breugel, W., Rengelink, R., & Jarvis, M. J. 2002, AJ, 123, 1784
- Devriendt, J. E. G., Guiderdoni, B., & Sadat, R. 1999, A&A, 350, 381
- Dey, A., Graham, J. R., Ivison, R. J., Smail, I., Wright, G. S., & Liu, M. C. 1999, ApJ, 519, 610

- Eisenhardt, P. R. & Wright, E. L. 2003, SPIE, 4850, 1050
- Elston, R. et al. 2004, in preparation
- Fan, X. et al. 2003, AJ, 125, 1649
- Fazio, G. G. et al. 2004, ApJS, this volume
- Fixsen, D. J., Moseley, S. H., & Arendt, R. G. 2000, ApJ, 128, 651
- Hogg, D. W., Neugebauer, G., Cohen, J. G., Dickinson, M., Djorgovski, S. G., Matthews, K., & Soifer, B. T. 2000, AJ, 119, 1519
- Huang, J., Cowie, L. L., Gardner, J. P., Hu, E. M., Songaila, A., & Wainscoat, R. J. 1997, ApJ, 476, 12
- Jannuzi, B. T. & Dey, A. 1999, in *Photometric Redshifts and High-Redshift Galaxies*, ed. R. Weymann, L. Storrie-Lombardi, M. Sawicki, & R. Brunner, Vol. 191 (San Francisco: ASP Conference Series), 111
- Jarrett, T. H., Chester, T., Cutri, R., Schneider, S. E., & Huchra, J. P. 2003, AJ, 125, 525
- Johnson, H. L. 1966, ARA&A, 4, 193
- Kenter, A. et al. 2004, in preparation
- Murray, S. S. et al. 2004, in preparation
- Polletta, M., Courvoisier, T. J., Hooper, E. J., & Wilkes, B. 2000, A&A, 362, 75
- Richards, G.T. et al. 2002, AJ, 123, 2945
- Sato, Y. et al. 2003, A&A, 405, 833
- van Dokkum, P. G., Franx, M., Fabricant, D., Illingworth, G. D., & Kelson, D. D. 2000, ApJ, 541, 95
- Vanden Berk, D. E. et al. 2001, AJ, 122, 549

Table 1. Properties of the IRAC Shallow Survey

λ (μm)	Area (\square°)	5σ 3'' (μJy)	5σ 3'' (Vega mag)	5σ 6'' (μJy)	5σ 6'' (Vega mag)	Saturation (Vega mag)
3.6	8.55	6.4	19.1	12.3	18.4	10.0
4.5	8.53	8.8	18.3	15.4	17.7	9.8
5.8	8.54	51	15.9	76	15.5	7.5
8.0	8.54	50	15.2	76	14.8	7.7



Fig. 1.— Mosaic $4.5\ \mu\text{m}$ image of the complete IRAC shallow survey, with N up and E left, subtending $\approx 2.92^\circ \times 3.54^\circ$. Insets highlight the galaxy group UGC9315 (at left in large central inset), NGC 5646 (lower right), the extreme $8\mu\text{m}$ to I flux ratio object IRAC J142939.1+353557 (upper left), and a region with a high density of sources with red $3.6\mu\text{m}$ - $4.5\mu\text{m}$ colors, suggestive of a $z > 1$ cluster (lower left). Blue, green, and red in the insets correspond to 3.6 , 4.5 , and $8\mu\text{m}$, except for the lower left where red is $4.5\mu\text{m}$ and green is the average of 3.6 and $4.5\mu\text{m}$.

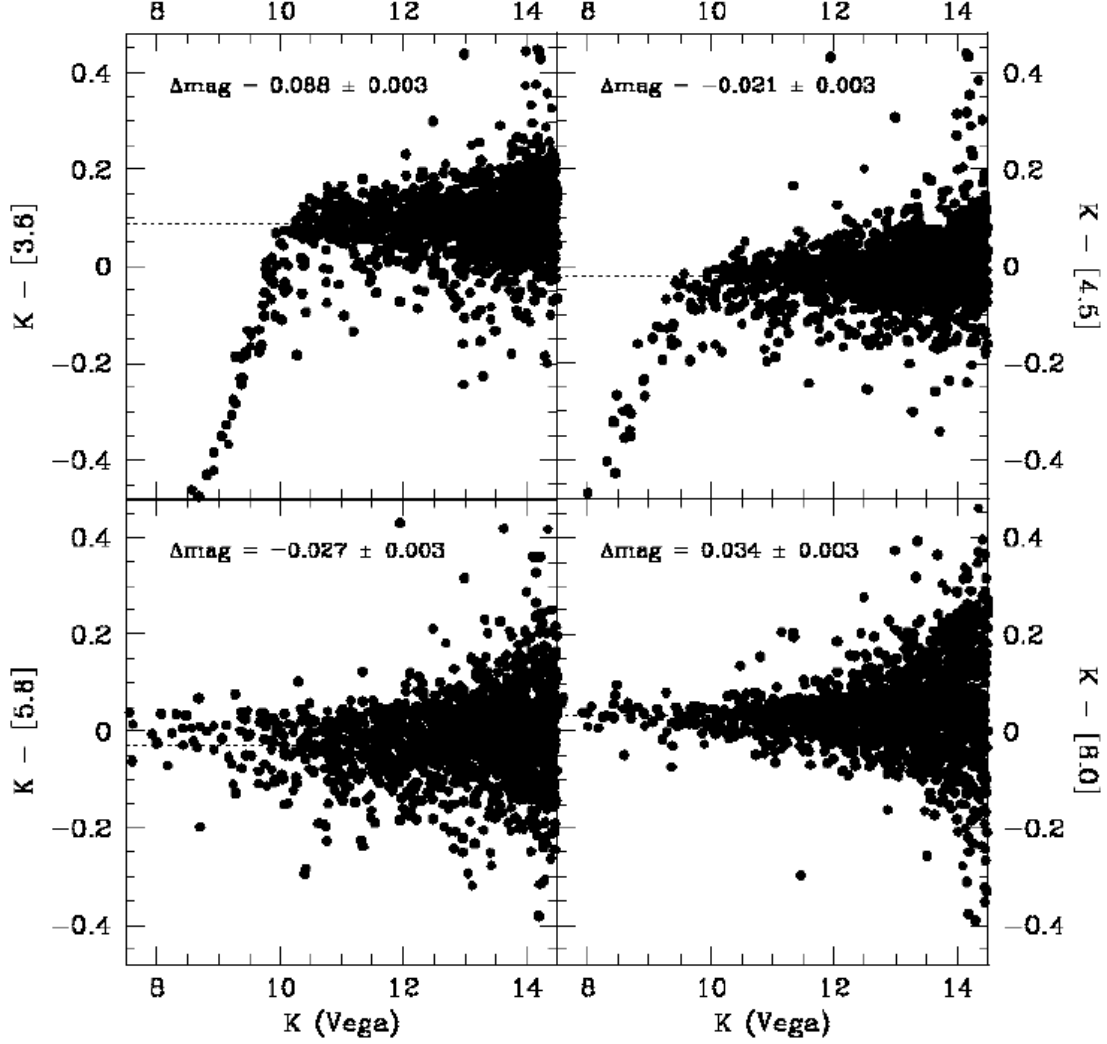


Fig. 2.— $K - \text{IRAC}$ versus K for 2MASS counterparts with $J - K \leq 0.5$. IRAC photometry is measured in $6''$ diameter apertures, corrected to 10 pixel radius ($24.4''$ diameter) apertures. The horizontal dotted lines show the average of the distribution for $10 < K < 13$. Saturation effects are apparent at 3.6 and $4.5\mu\text{m}$ for sources with $K < 10$.

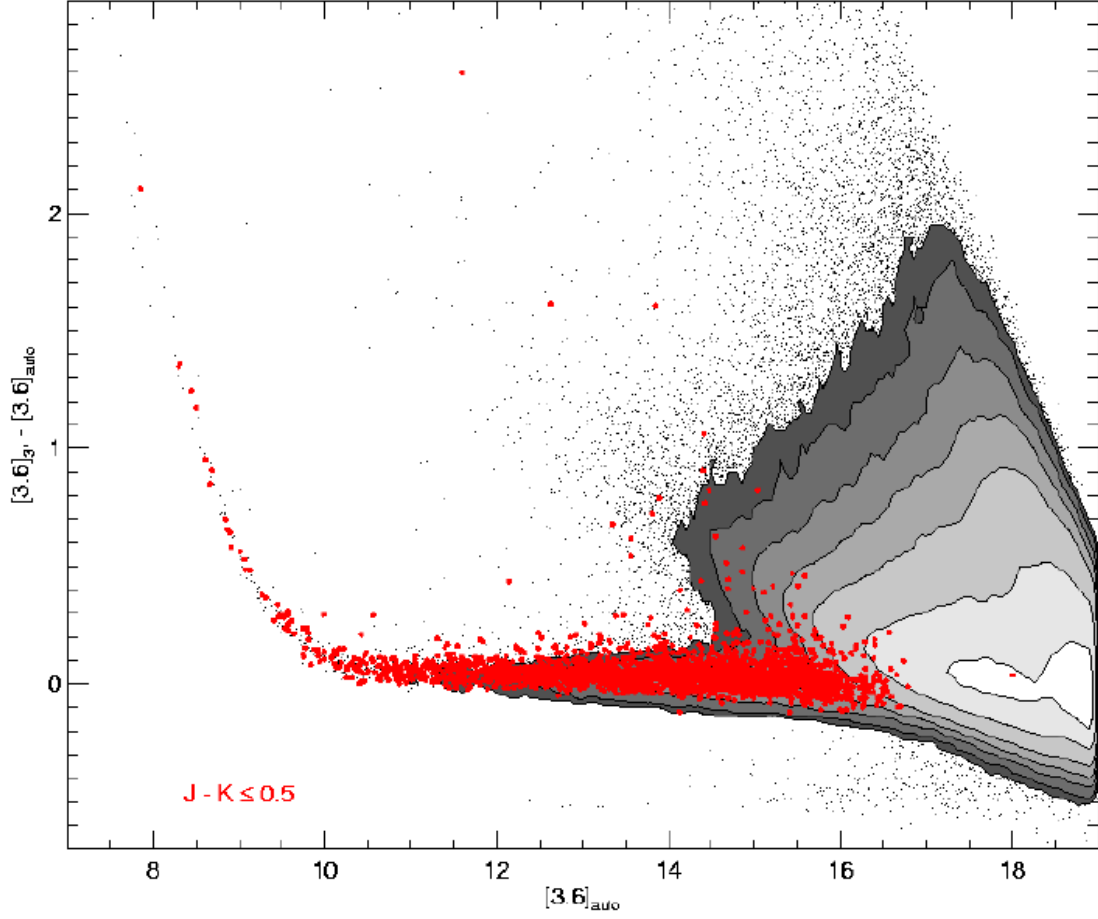


Fig. 3.— Concentration parameter $[3.6]_{3''} - [3.6]_{\text{auto}}$ versus $[3.6]_{\text{auto}}$, where $[3.6]_{3''}$ is the SExtractor-derived flux of sources in $3''$ diameter apertures, corrected to $24.4''$ apertures, and $[3.6]_{\text{auto}}$ is the SExtractor-derived MagAuto. Progressively lighter shaded contours separate regions at surface densities of $[2, 5, 10, 20, 50, 100] \times 10^3$ objects per mag per mag. Red points indicate 2MASS counterparts with $J - K \leq 0.5$, which is a robust selection criterion for Galactic stars.

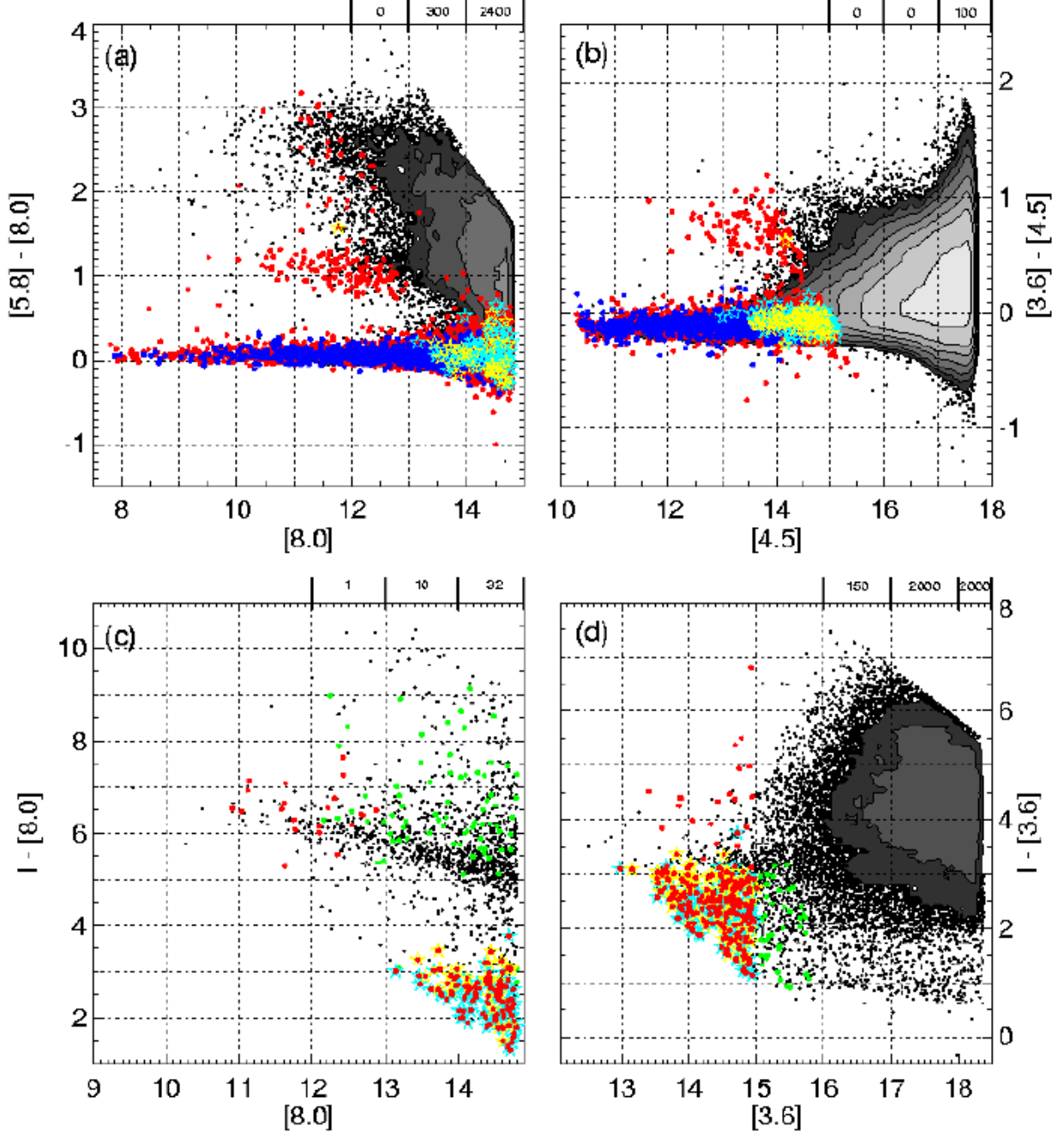


Fig. 4.— Color-magnitude relations for IRAC shallow survey and released NDWFS Boötes data. Objects were required to be fainter than the saturation limits and brighter than the $6''$ 5σ limits in Table 1 in the selection band (horizontal axis), and above 2σ in the bluer band in order to be plotted. The numbers of objects redder than the 2σ limits are listed along the top axes as a function of magnitude. Progressively lighter shaded contours separate regions at surface densities of $[1, 2, 5, 10, 20, 50, 100] \times 10^3$ objects per mag per mag. Objects classified as stars based on the $3.6\mu\text{m}$ concentration are plotted as red, while objects with $2MASS\ J - K \leq 0.5$ are plotted as blue. Objects identified as dwarf stars in Fig. 5a appear

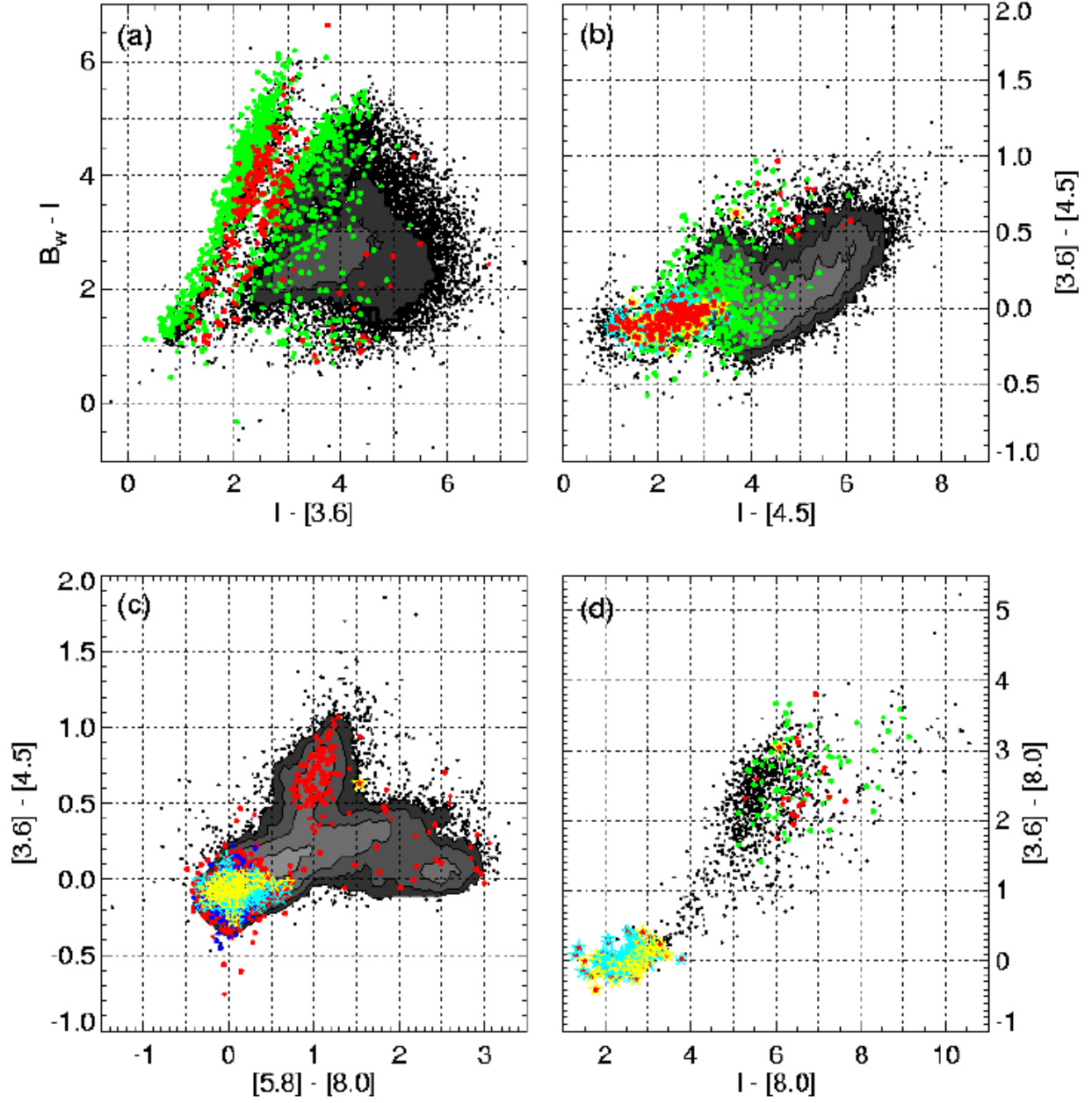


Fig. 5.— Color-color relations for IRAC shallow survey and released NDWFS Boötes data. Objects are detected at or above 5σ in all bands plotted. Shaded contour levels and symbol colors are the same as in figure 4.

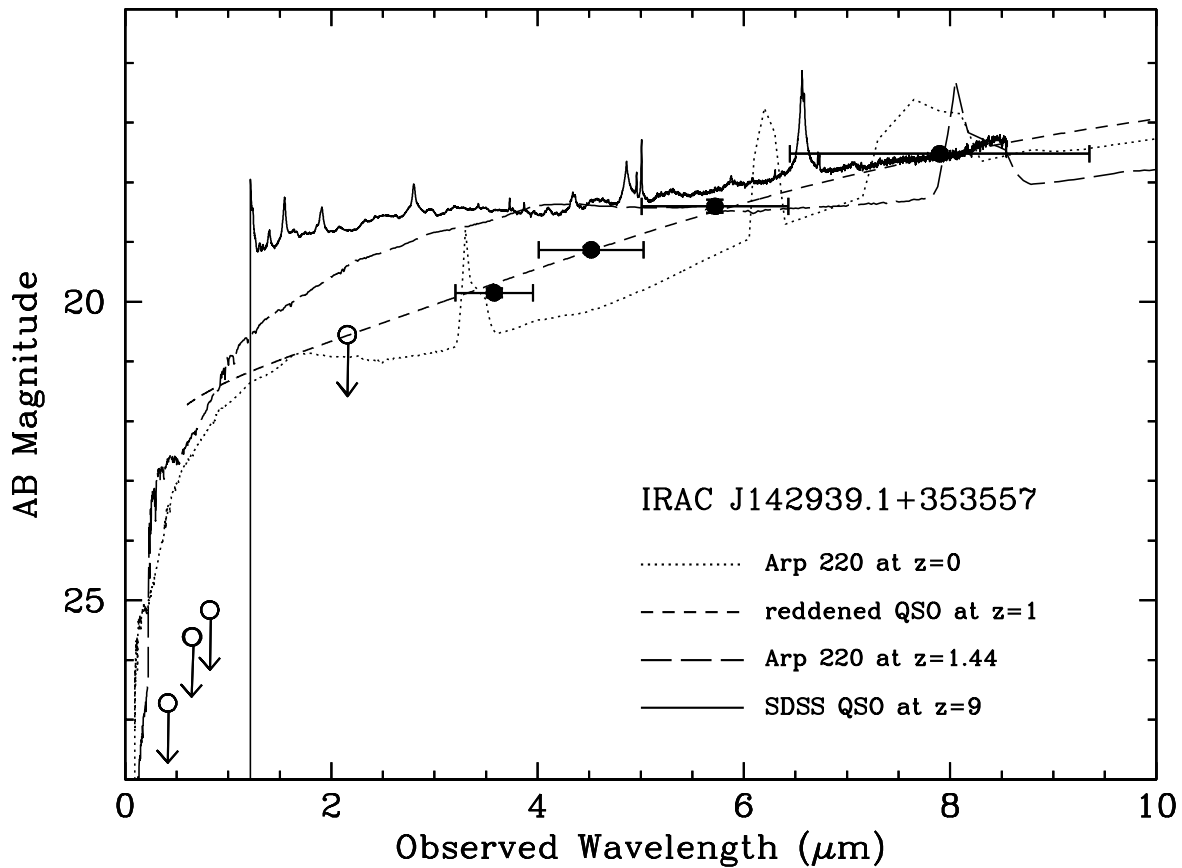


Fig. 6.— Observed fluxes for IRAC J142939.1+353557, an object with an extreme ratio of $8\mu\text{m}$ to I flux. Models are explained in the text.